ACS Partner Journal

CHEMICAL & BIOMEDICAL IMAGING

pubs.acs.org/ChemBioImaging

Article

Nonemissive Iridium(III) Solvent Complex as a Self-Reporting Photosensitizer for Monitoring Phototherapeutic Efficacy in a "Signal on" Mode

Manping Qian,[#] Ke Wang,[#] Peng Yang, Yu Liu, Meng Li,* Chengxiao Zhang, and Honglan Qi*

Cite This: *Chem. Biomed. Imaging* 2024, 2, 808−816

Read Online

ACCESS | Metrics & More | Article Recommendations | Supporting Information

ABSTRACT: Photodynamic therapy (PDT) has long been receiving increasing attention for the minimally invasive treatment of cancer. The performance of PDT depends on the photophysical and biological properties of photosensitizers (PSs). The always-on fluorescence signal of conventional PSs makes it difficult to real-time monitor phototherapeutic efficacy in the PDT process. Therefore, functional PSs with good photodynamic therapy effect and self-reporting properties are highly desired. Here, two nonemissive iridium(III) solvent complexes, $[(dfppy)_2Ir(DMSO)]Cl$ (Ir-DMSO, dfppy = 2,4-difluorophenyl)pyridine, DMSO = dimethyl sulfoxide) and $[(dfppy)_2Ir(ACN)]Cl$ (Ir-ACN, ACN = acetonitrile) as PSs, were synthesized. Both of them exhibit intense high-energy absorption bands, low photoluminescence (PL) emission, and low dark toxicity. Thanks to the lower dark toxicity of Ir-DMSO, we chose it as a PS for further PDT. In this work, Ir-DMSO functions as a specific PL "signal on" PS for self-reporting therapeutic efficacy during its own PDT process. Colocalization experiments indicated that Ir-DMSO accumulated in the endoplasmic reticulum and mitochondria. Under light irradiation, Ir-DMSO not only exhibited the ability to kill cancer cells but also presented a "signal on" PL response toward cell death. During Ir-DMSO-induced PDT, cell death modality was further investigated and immunogenic cell death was revealed, in which main hallmarks, including ROS generation, upregulation of surface-exposed calreticulin, high-mobility group box 1, and adenosine triphosphate secretion, were observed. Thanks to the specific coordination reaction between Ir-DMSO and histidine (His)/His-containing proteins, the phototherapeutic efficacy can be monitored in real time without other signal probes. This work provides a new and promising strategy for the development of PSs with self-reporting ability, which is of great importance for imaging-guided PDT.

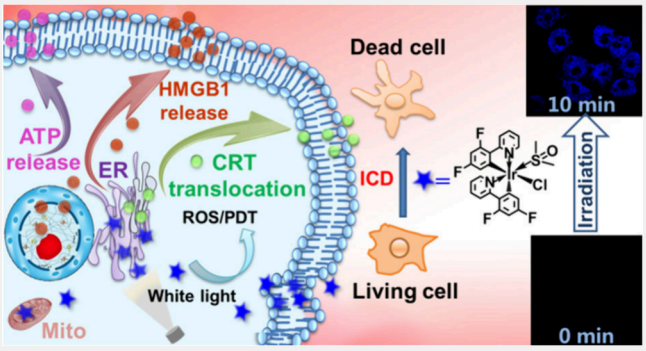

KEYWORDS: *Iridium(III) solvent complex, Self-reporting photosensitizer, Phototherapeutic efficacy, Signal on, Immunogenic cell death*

INTRODUCTION

Cancer is a major cause of global mortality with great effect on life quality.[1] So much effort has been made to develop effective diagnostic and therapeutic techniques.[2,3] In recent years, photodynamic therapy (PDT) has become a hopeful technology for cancer treatment due to the distinctive benefits of noninvasive therapy, high specificity, controllability, and high spatiotemporal precision.[4,5] PDT is a photochemical-based treatment approach that involves the use of photosensitizers (PSs) to produce highly cytotoxic reactive oxygen species (ROS) upon light irradiation for inducing cancer cell death.[6] A wide range of PSs has been developed, such as organic fluorophores, transition metal complexes, and nanomaterials.[7−12] Despite good PDT efficacy, the conventional PSs cannot real-time monitor the phototherapeutic effect, which leads to problems such as overtreatment or delay of treatment during the PDT process.[13,14] Therefore, the development of new PSs with good photodynamic therapy efficacy and self-reporting properties is highly desired.

Self-reporting PSs with the ability to produce ROS and monitor ROS production or therapeutic efficiency simultaneously have recently emerged as promising candidates in PDT.[15−17] PSs with a self-reporting capacity present obvious visualization of the phototheranostic process;[17] thus, excessive phototoxicity and other adverse effects caused by irradiation and drug toxicity can be significantly mitigated. In present, PSs with self-reporting ability are mainly designed based on small

Received: May 7, 2024
Revised: July 8, 2024
Accepted: July 23, 2024
Published: August 1, 2024

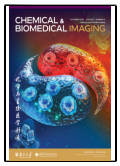

organic compounds, which are usually modified with activable groups.[18] The unique features of iridium(III) complexes provide new opportunities for the facile design of self-reporting probes with improved therapeutic accuracy and efficacy for image-guided PDT. However, to the best of our knowledge, there is no report on iridium(III) complexes as self-reporting PSs to monitor therapeutic efficacy during image-guided PDT.

Herein, we designed and synthesized two small molecular PSs by introducing organic solvents (dimethyl sulfoxide (DMSO) and acetonitrile (ACN)) into iridium(III) complexes as auxiliary ligands. The photophysical properties and in vitro cytotoxicity of the two iridium(III) solvent complexes were investigated. Ir-DMSO with lower dark cytotoxicity was utilized as a self-reporting PS for monitoring phototherapeutic efficacy, as shown in Scheme 1. Under white light irradiation,

Scheme 1. (A) Synthetic Route of Ir-DMSO; (B) Schematic Illustration of Ir-DMSO as "Signal on" Self-Reporting PS for Real-Time Monitoring of Therapeutic Efficacy During PDT

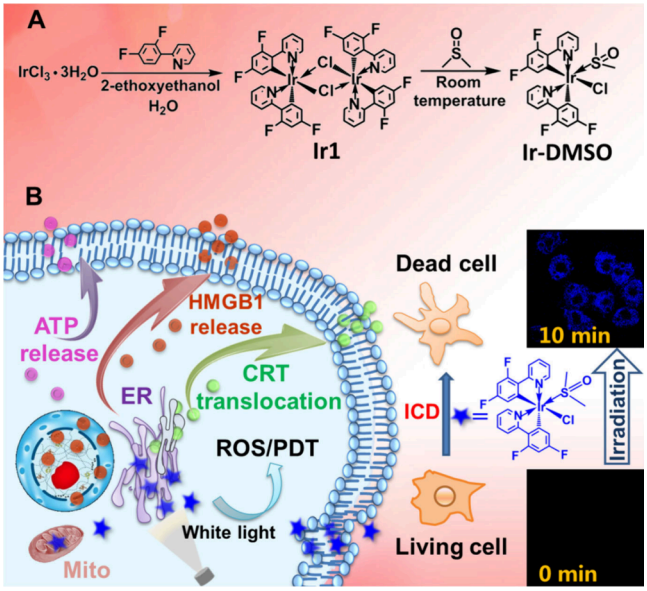

Ir-DMSO not only exhibited the ability to eradicate cancer cells, but also to self-indicate cell demise through photoluminescence (PL) emission enhancement. Cell death modality during Ir-DMSO induced PDT was further investigated and immunogenic cell death (ICD) was identified, in which the main hallmarks, including ROS generation, upregulation of surface-exposed calreticulin (CRT), high-mobility group box 1 (HMGB1), and adenosine triphosphate (ATP) release, were observed. Particularly, the self-reporting property of Ir-DMSO through its own PDT was finally confirmed, and phototherapeutic efficacy can be monitored in real time without other signal probes, exhibiting great potential for image-guided PDT.

EXPERIMENTAL SECTION

Material and Apparatus

$IrCl_3 \cdot 3H_2O$ was purchased from Xi'an Shengyi New Material Technology Co., Ltd. (China). 2-(2,4-Difluorophenyl)pyridine (dfppy), DMSO, ACN, and 2-ethoxyethanol were ordered from J&K Scientific Ltd. (China). Diethyl pyrocarbonate (DEPC) and Cell Counting Kit-8 (CCK-8) were purchased from Beijing Solarbio Science & Technology Co., Ltd. (China). 2,7-Dichlorodihydrofluorescein diacetate (DCFH-DA), methylene blue, and 2,2,6,6-tetramethylpiperidine (TEMP) were obtained from TCI Corporation (China). Endoplasmic reticulum specific fluorescent dye (ER-Tracker Red, ERTR), mitochondria specific fluorescent dye (Mito-Tracker Red, MTR), lysosome specific fluorescent dye (Lyso-Tracker Red, LTR), Annexin V-FITC/propidium iodide (PI) double staining kit were purchased from Biotech. Inc. (China). Calcein Acetoxymethyl Ester (Calcein-AM) was supplied by Dojindo Laboratories (Japan). Alexa Fluor 555 conjugate antirabbit IgG (H+L), alexa Fluor 488 conjugate CRT rabbit mAb, HMGB1 antibody and ATP assay kit were purchased from Cell Signaling Technology (U.S.A.). Confocal laser scanning microscope (CLSM) images system (FV1200, Olympus, Japan), UV−visible spectrophotometer (UV-2450, Shimadzu Corporation, Japan), and fluorescence spectrophotometer (Fluorolog-3, Horiba JY, Japan) were used in this work for characterization and measurements.

Synthesis of Ir-DMSO and Ir-ACN

Ir-DMSO and Ir-ACN were synthesized according to the synthetic route shown in Scheme S1, and details are presented in the Supporting Information.

Cytotoxicity

To test the cytotoxicity of Ir-DMSO and Ir-ACN, 100 μL of the freshly cultured HeLa cell medium with a density of 1×10^5 cells/mL was added into a 96-well plate cultivated at 37 °C for 24 h under a 5% CO_2 atmosphere. After that, HeLa cells were further cultured in 100 μL of culture medium containing different concentrations of Ir-DMSO or Ir-ACN for 30 min. And then, the wells containing the resulting cells were separated into two groups. One group was irradiated with white light (20 mW/cm^2) for 10 min, while another group was kept in the dark for 10 min, and then all groups were further cultivated in the dark for 24 h. After extracting the medium, the cells were washed twice with PBS. Then 10 μL of the original CCK-8 solution and 100 μL of PBS were dropped into each well, and the wells were further incubated at 37 °C for 4 h. Finally, the cytotoxicity of the sample to HeLa cells was calculated on the basis of the absorbance at 450 nm.

PDT Experiment

For PDT testing, HeLa cells were first treated with 10 μM Ir-DMSO for 30 min at 37 °C. Followed by washing with PBS, the resulting HeLa cells were then cultured in fresh culture medium under white light irradiation (20 mW/cm^2) for different amounts of time. After exposure to white light, the processed cells were further treated with Calcein-AM and PI for 30 min or Annexin V-FITC and PI for 30 min, respectively, followed by PBS washing. For CLSM imaging, there was no phenol red in the cell culture medium. The CLSM images were collected within windows of 450−550 nm, with an excitation wavelength at 405 nm for Ir-DMSO, 500−550 nm with an excitation wavelength at 488 nm for Annexin V-FITC and Calcein-AM, and 570−670 nm with an excitation wavelength at 559 nm for PI.

RESULTS AND DISCUSSION

Design and Synthesis

Dfppy was usually used as the main ligand of blue light iridium(III) complexes. For iridium(III) complexes using dfppy as the main ligand, interligand energy transfer (ILET)[19] could occur from the higher level dfppy-centered triplet metal-to-ligand charge transfer (^{3}MLCT) state to the auxiliary ligand-centered ^{3}MLCT or auxiliary ligand center (^{3}LC) state. PL emission mainly came from auxiliary ligand-dominated ^{3}MLCT/^{3}LC, so emission properties of the iridium(III) complex can be modulated through auxiliary ligands. In this work, organic solvent (DMSO or ACN) was introduced to the molecular structure of the iridium(III) complex via two-step reactions to produce iridium(III) solvent

https://doi.org/10.1021/cbmi.4c00042
Chem. Biomed. Imaging 2024, 2, 808−816

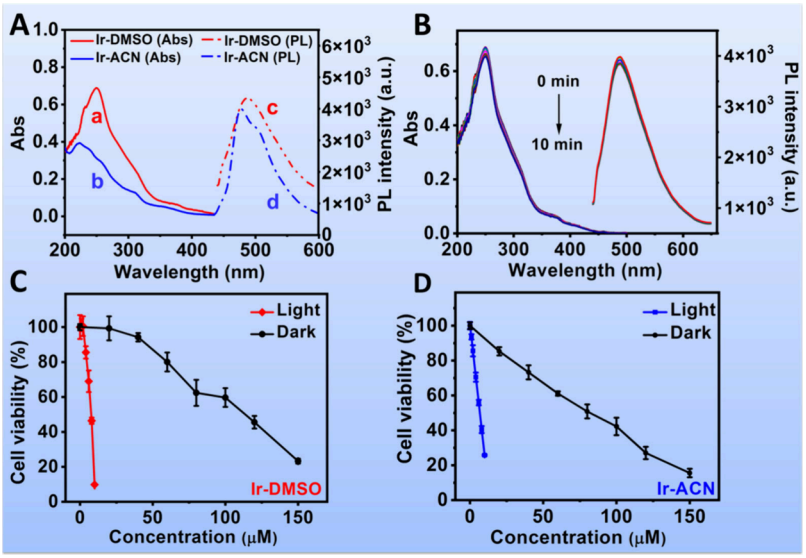

Figure 1. (A) UV−vis absorption spectra (solid line) and PL emission spectra (dotted line) of 10 μM of Ir-DMSO (λ_{ex} = 375 nm) and Ir-ACN (λ_{ex} = 355 nm) in 0.01 M PB-DMSO (v/v = 99:1). (B) UV−vis absorption spectra and PL emission spectra of Ir-DMSO in 0.01 M PB-DMSO (v/v = 99:1) under white light irradiation (20 mW/cm^2) for different times. (C,D) Cell viability (%) of HeLa cells against different concentrations of Ir-DMSO (C) or Ir-ACN (D) under dark or white light irradiation (20 mW/cm^2, 10 min).

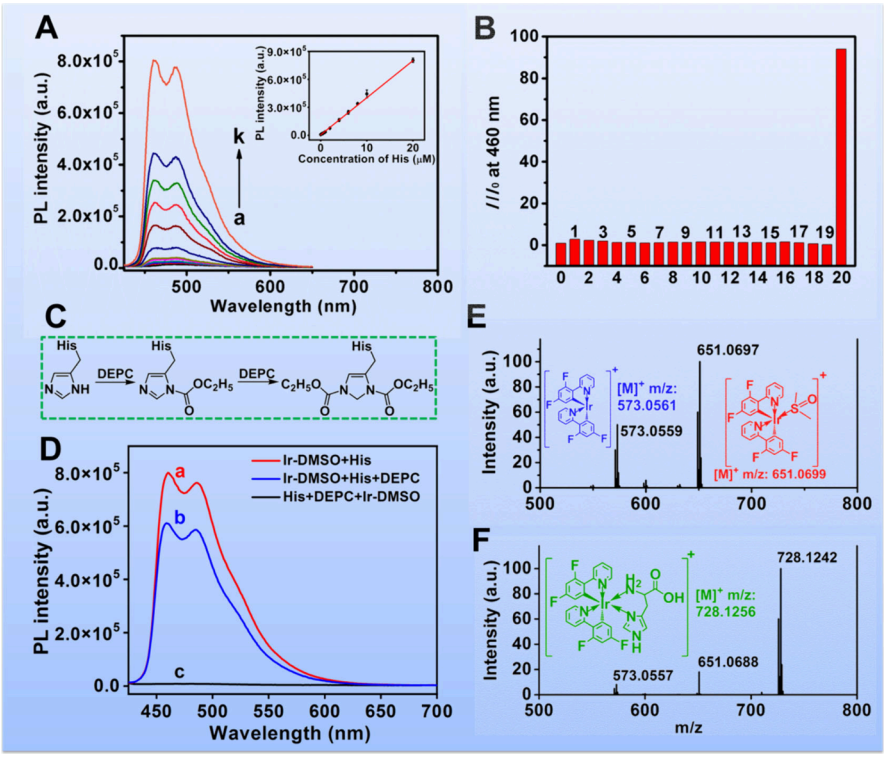

Figure 2. (A) PL emission spectra of 5.0 μM Ir-DMSO in the presence of His (a−k, 0.2, 0.4, 0.6, 0.8, 1.0, 2.0, 4.0, 6.0, 8.0, 10, 20 μM, respectively); inset, calibration curve of His. (B) The relative PL intensity I/I_0 of 5.0 μM Ir-DMSO in the presence of 20 μM His and 100 μM of the other 19 natural amino acids in aqueous solution for 30 min, λ_{ex} = 375 nm, λ_{em} = 460 nm. I_0 represents the PL intensity of Ir-DMSO only. I represents the PL intensity of Ir-DMSO in the presence of various amino acids (0, blank; 1, L-methionine; 2, L-serine; 3, L-lysine; 4, L-leucine; 5, L-alanine; 6, L-isoleucine; 7, L-valine; 8, L-arginine; 9, L-glycine; 10, L-cysteine; 11, L-tryptophan; 12, L-glutamine; 13, L-aspartic acid; 14, L-phenylalanine; 15, L-proline; 16, L-tyrosine; 17, L-asparagine; 18, L-threonine; 19, L-glutamic; 20, L-histidine). (C) Reaction pathway of the histidine-imidazole group with an excess of DEPC. (D) PL emission spectra of Ir-DMSO under different conditions (a, 5.0 μM Ir-DMSO + 20 μM His; b, 0.1 mM DEPC adding into the mixture of 5.0 μM Ir-DMSO + 20 μM His; c, 5.0 μM Ir-DMSO adding into the mixture of 20 μM His + 0.1 mM DEPC). (E) ESI-HRMS spectrum of Ir-DMSO. (F) ESI-HRMS spectrum of Ir-DMSO with 1 equiv of His.

complex, as shown in Scheme S1. First, chloro-bridged iridium(III) dimer $[(dfppy)_2Ir(\mu\text{-}Cl)]_2$ (Ir1) was synthesized[20] by mixing and refluxing $IrCl_3 \bullet 3H_2O$ and dfppy in the mixture solvent of 2-ethoxyethanol/H_2O. Then Ir1 was dissolved in DMSO and stirred for 30 min at room temperature under N_2 atmosphere. The chemical structure of Ir1 was characterized

https://doi.org/10.1021/cbmi.4c00042
Chem. Biomed. Imaging 2024, 2, 808−816

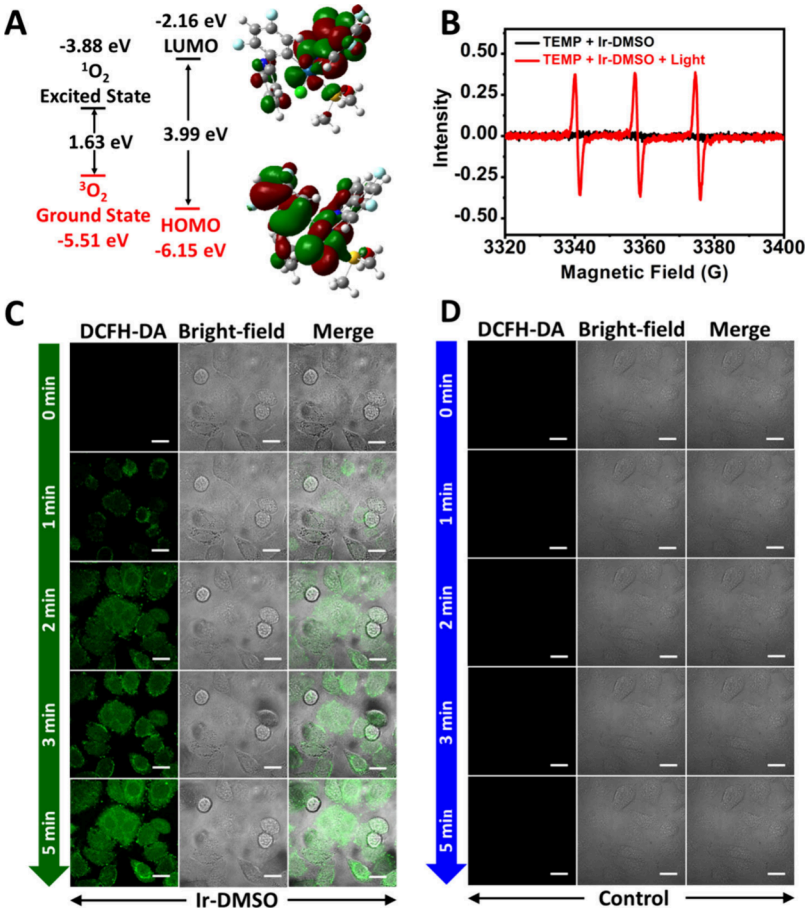

Figure 3. (A) Energy level of Ir-DMSO and ground state oxygen ($^3O_2$) absorption. The HOMO and LUMO of Ir-DMSO were calculated by DFT using CAM-B3LYP/6-31G* and LANL2DZ. (B) ESR spectra of Ir-DMSO trapped by TEMP in 0.01 M PB-DMSO (v/v = 99:1) with/without white light irradiation (20 mW/cm^2) for 10 min. (C,D) CLSM images of HeLa cells after incubation with 20 μM DCFH-DA and 10 μM Ir-DMSO (C), and only 20 μM DCFH-DA (D) under white light irradiation (20 mW/cm^2) for different times. Scale bar: 20 μm.

by nuclear magnetic resonance hydrogen spectroscopy (^{1}H NMR, Figure S1), ^{1}H−^{1}H correlation spectroscopy NMR (^{1}H−^{1}H COSY, Figure S2), and electrospray ionization with high-resolution mass spectrometry (ESI-HRMS, Figure S3). ^{1}H NMR identified and quantified hydrogen atom types and quantities of Ir1 (Figure S1) and ^{1}H−^{1}H COSY NMR further confirmed correlations between the hydrogen atoms in Ir1 (Figure S2). The ESI-HRMS features a major peak centered at m/z [M]$^+$ 573.0550 (calculated, 573.0561) for Ir1 (Figure S3), indicating the successful synthesis of Ir1. Then the chemical structure of Ir-DMSO was verified by ESI-HRMS (Figure S4), from which a major peak centered at m/z [M]$^+$ 651.0697 (calculated, 651.0699). In addition, the structure of Ir-DMSO was further confirmed by single-crystal X-ray crystallographs. The details of the experimental conditions, unit cell data, and refinement data are summarized in Figure S5 and Tables S1−S3. Ir-DMSO forms orthorhombic, and the Ir atom coordinates the N atoms from two dfppy ligands and the S atom of DMSO and Cl anion (Figure S5 and Table S2). Ir-ACN was also synthesized by choosing ACN as another solvent ligand and characterized by ESI-HRMS. A major peak centered at m/z [M]$^+$ 614.0827 (calculated, 614.0827) in ESI-HRMS (Figure S6), indicating the successful synthesis of Ir-ACN.

Photophysical and Biological Properties

The UV−vis absorption spectra and PL emission spectra of Ir-DMSO and Ir-ACN in 0.01 M PB-DMSO (v/v = 99:1) are shown in Figure 1A. Both of them display intense high-energy absorption bands from 230 to 340 nm and weak absorption bands from 340 to 470 nm (Figure 1A, solid line), which are similar to the typical iridium(III) complex.[20] The corresponding molar extinction coefficients (ε) were then calculated to be 6.84×10^4 M^{-1} cm^{-1} at 375 nm for Ir-DMSO and 5.53×10^4 M^{-1} cm^{-1} at 355 nm for Ir-ACN, both of which were higher than the hematoporphyrin derivative (HPD)[21] and other reported iridium(III) complex PSs.[15,17] These results indicate the strong absorption ability of the two iridium(III) solvent complexes in the corresponding spectral region. Meanwhile, PL behavior shows that the two iridium(III) solvent complexes have a weak PL emission with a maximum emission wavelength at 488 nm for Ir-DMSO (Figure 1A,c) and 478 nm for Ir-ACN (Figure 1A,d), respectively. Also, extremely low PL quantum yields (Φ < 0.01%) were obtained for the two PSs. In addition, upon white light irradiation (20 mW/cm^2), the absorption spectra and PL emission spectra of Ir-DMSO and Ir-ACN show almost no change, manifesting their good photostability (Figures 1B and S7).

The dark cytotoxicity and phototoxicity of Ir-DMSO and Ir-ACN to HeLa cells were examined by the CCK-8 method. The IC_{50} values of Ir-DMSO and Ir-ACN in the dark were 118.8

https://doi.org/10.1021/cbmi.4c00042
Chem. Biomed. Imaging 2024, 2, 808−816

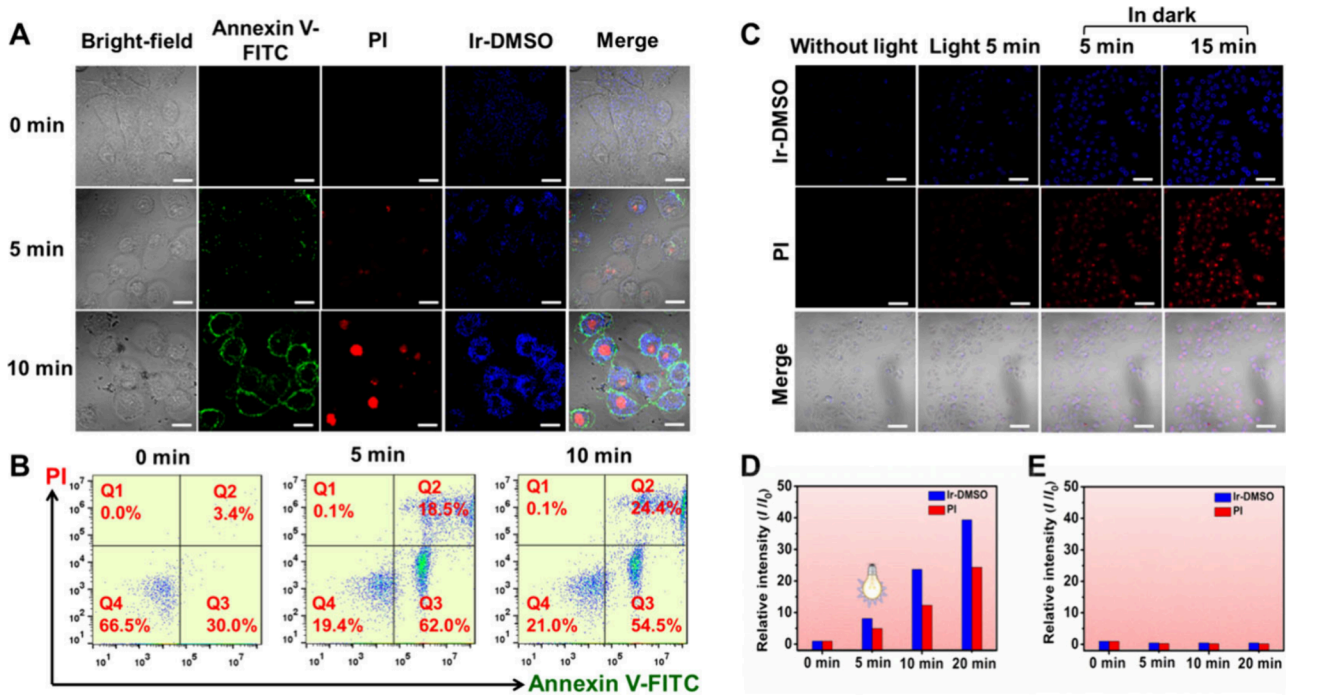

Figure 4. (A) CLSM images and (B) flow cytometry results of HeLa cells treated with different processes. HeLa cells were first incubated with Ir-DMSO (10 μM, 30 min) and then irradiated without or with white light irradiation (20 mW/cm^2) for 5 and 10 min, respectively. Then, all HeLa cells were incubated with Annexin V-FITC and PI for 30 min. Scale bar: 10 μm. (C) CLSM images of HeLa cells costained with Ir-DMSO and PI treated with different processes. Scale bar: 100 μm. (D) The relative emission intensity of Ir-DMSO and PI in HeLa cells placed in the dark for different times after light irradiation for 5 min. (E) The relative emission intensity of Ir-DMSO and PI in HeLa cells at different times without light irradiation.

and 81.3 μM, respectively (Figure 1C,D). Moreover, upon white light irradiation (20 mW/cm^2, 10 min), cell viability was greatly reduced, the values of IC_{50} under light exposure were 7.7 and 6.4 μM (Figure 1C,D), and the phototoxicity indexes were 15.4 and 12.7 for Ir-DMSO and Ir-ACN, respectively. Lower dark cytotoxicity and strong phototoxicity of Ir-DMSO were obtained compared with that of Ir-ACN. Therefore, Ir-DMSO was chosen as a PS for further PDT in the following experiments.

Inspired by the specific luminescent properties of $[Ir(ppy)_2(solv)_2]^+$ (ppy = 2-phenylpyridine, solv = H_2O or CH_3CN) for histidine (His)/His-rich proteins,[22] here we investigated interactions between Ir-DMSO and biomolecules, including amino acids or proteins, bases, or DNA. As shown in Figure 2A, two PL emission peaks with wavelengths at 460 and 488 nm were observed for Ir-DMSO in the presence of His, and their relative PL intensities increased linearly with the His concentration within the range of 0.2−20 μM. In contrast, there was nearly no PL emission for the other 19 amino acids (Figure 2B), which demonstrates the specific PL-enhanced response of Ir-DMSO to His. After diethyl pyrocarbonate (DEPC, a His-specific alkylating reagent, Figure 2C)[23] was added in the solution, PL responses of Ir-DMSO-His decreased (Figure 2D,b). In particular, Ir-DMSO displays nearly no signal when added into the mixture of DEPC-His adducts (Figure 2D,c), indicating that the enhanced PL comes from the interaction between Ir-DMSO and His. Responses of Ir-DMSO to polypeptides and proteins containing different numbers of His residues were further explored and shown in Figure S8. As expected, PL signal enhancements to varying degrees were observed. In addition, we found that bases ss-DNA and ds-DNA did not influence the PL response of Ir-DMSO compared with that of His (Figure S9).

To further confirm the interaction between Ir-DMSO and His, ESI-HRMS of Ir-DMSO with different amounts of His was conducted. As shown in Figure 2E, Ir-DMSO in CH_3OH showed two major peaks centered at 573.0559 and 651.0697, corresponding to $[(dfppy)_2Ir]^+$ (calculated, 573.0561) and $[(dfppy)_2Ir(DMSO)]^+$ (calculated, 651.0699), respectively. When adding 1 or 2 equiv of His, major peaks centered at 728.1242 and 728.1258 can be clearly observed, which can be ascribed to $[(dfppy)_2Ir(His)]^+$ (calculated, 728.1256) (Figures 2F, S10, and S11). For 1 equiv of His, major peaks corresponding to $[(dfppy)_2Ir]^+$ (573.0557) and $[(dfppy)_2Ir(DMSO)]^+$ (651.0688) can still be clearly observed (Figure 2F), while 2 equiv of His caused disappearance of characteristic peaks of $[(dfppy)_2Ir]^+$ and $[(dfppy)_2Ir(DMSO)]^+$ (Figure S10), indicating that Ir-DMSO indeed react with His. Another two small new peaks centered at 156.0771 and 883.1956 were observed, which corresponded to $[(His) + H]^+$ (calculated, 156.0768) and $[(dfppy)_2Ir(His)_2]^+$ (calculated, 883.1951), respectively (Figures S10 and S12). Together, these results demonstrate that Ir-DMSO can specifically identify His and His-containing peptide/proteins by reacting with the imidazole ring of His species.

Subcellular Localization Investigation

The subcellular localization of Ir-DMSO in HeLa cells was studied by colocalization experiments using ERTR, MTR, and LTR. Because of weak-emission of Ir-DMSO inside HeLa cells, His was added after HeLa cells were treated with Ir-DMSO according to previous work.[24] As shown in Figure S13, bright blue PL emissions of Ir-DMSO-His were overlapped with that

https://doi.org/10.1021/cbmi.4c00042
Chem. Biomed. Imaging 2024, 2, 808−816

of ERTR and Pearson's coefficient was calculated to be 0.8947. Meanwhile, Pearson's coefficients of Ir-DMSO-His with MTR and LTR were 0.8822 and 0.3760, respectively, suggesting that Ir-DMSO was predominantly accumulated in endoplasmic reticulum (ER) and mitochondria (Mito).

ROS Generation Ability

To evaluate ability of $^1O_2$ generation for Ir-DMSO, we first used density functional theory (DFT) to compute molecular orbital energy level of Ir-DMSO. From Figure 3A we know that the highest occupied molecular orbital (HOMO) and lowest unoccupied molecular orbital (LUMO) of Ir-DMSO are −6.15 and −2.16 eV, respectively. Thus, the band gap of Ir-DMSO (3.99 eV) was overlapped with that of $^1O_2$ (1.63 eV),[25] indicating that Ir-DMSO could have the ability to generate $^1O_2$ (Figure 3A). The type of ROS produced by Ir-DMSO upon white light irradiation was checked by electron spin resonance (ESR) spectroscopy. A characteristic $^1O_2$ induced triplet signal was obviously shown, while no characteristic signal of $^{\bullet}$OOH or $^{\bullet}$OH radicals was observed (Figure 3B). Using 1,3-diphenylisobenzofuran (DPBF) as a $^1O_2$ indicator and methylene blue as a reference, the $^1O_2$ yield of Ir-DMSO was calculated to be 0.45 (Figure S14), which is much higher than Photofrin (Φ = 0.25) and Foscan (Φ = 0.31).[26]

The ROS generation ability of Ir-DMSO in live cells was further investigated using 2,7-dichlorofluorescein diacetate (DCFH-DA) as an indicator. When ROS exists, DCFH-DA will be oxidized with a green fluorescence emission. As shown in Figure 3C, without white light irradiation, no green fluorescence emissions were observed from HeLa cells treated with Ir-DMSO. Upon white light irradiation (20 mW/cm^2), green fluorescence emissions can be clearly observed and the fluorescence intensity grew fast with the extension of light irradiation (Figure 3C). As a control, no fluorescence emissions were observed from HeLa cells treated with only DCFH-DA under the same conditions (Figure 3D). These results confirmed that Ir-DMSO possesses the outstanding ability to produce intracellular ROS under white light irradiation.

PDT Efficacy Evaluation

To evaluate the PDT effect of Ir-DMSO for the treatment of cancer cells, HeLa cells were exposed to 20 mW/cm^2 white light with different times after being treated with Ir-DMSO for 30 min, and cell viabilities were determined after irradiation via Annexin V-FITC (early apoptotic cells probe, green)/PI (necrotic cells or late-stage apoptotic cells probe, red) double staining kit and Calcein-AM (living cell probe, green)/PI double staining kit. As shown in Figure 4A, there are distinct fluorescence emissions from Annexin V-FITC for HeLa cells under light irradiation with different times. Without light irradiation, there are only bright green fluorescence emissions from Calcein-AM in the whole cells and no fluorescence emissions from PI (Figure S15A), showing that HeLa cells were live. After light irradiation for 5 min, there were weak discrete green fluorescence emissions from Annexin V-FITC on cell membrane along with membrane blebbing, and little red fluorescence emissions from PI within cells, indicating that these cells were at early stage of apoptosis. After irradiation for 10 min, there were strong intact green fluorescence emissions from Annexin V-FITC and red fluorescence emissions from PI, suggesting HeLa cells were at the late stage of apoptotic or necrotic (Figures 4A and S15). Also, the morphology and structure of HeLa cells changed during Ir-DMSO-induced PDT. In contrast, after a 10 min light irradiation without Ir-DMSO, there were green fluorescence emissions from Calcein-AM with normal cell morphology (Figure S15E). Meanwhile, flow cytometry analysis was performed with an Annexin V-FITC/PI apoptosis detection kit to further verify the PDT efficacy. As shown in Figure 4B, percentages of apoptotic and necrotic HeLa cells obviously increase with light exposure time, strongly confirming the PDT efficacy of Ir-DMSO for the treatment of cancer cells.

Self-Feedback of Phototherapeutic Efficacy

Self-reporting property of Ir-DMSO was finally investigated through its own PDT process, and time-dependent blue fluorescence emissions were recorded to monitor Ir-DMSO-induced cell death. As illustrated in Figure 4A, very weak blue fluorescence emitted only from cytoplasm after light irradiation for 5 min. With prolonged irradiation, strong blue fluorescence emissions were observed in the cytoplasm. When light irradiation increased to 20 min, strong blue fluorescence emissions were observed from the whole cells (Figure S15D). On the other hand, cell shrinkage and numerous membrane blebbing occurred after light irradiation, together with enhanced blue fluorescence with extended incubation time. Besides, through the change of blue luminescence emissions, the therapeutic effect of Ir-DMSO in its own PDT process can be real-time monitored. As shown in Figure 4C,D, the relative fluorescence intensity of Ir-DMSO and PI in each set of cells increased with light exposure time and Ir-DMSO exhibited greater signal variation than PI. As control, there is nearly no change in the fluorescence emission at different times without light irradiation (Figure 4E). Additionally, the possibility whether Ir-DMSO can be employed as an apoptosis indicator by enhanced blue fluorescence emissions when cisplatin was used to induce cell apoptosis was conducted. Strong blue fluorescence emissions appeared from HeLa cells treated with cisplatin and Ir-DMSO without light irradiation, accompanied by swollen nuclei, integrated nuclear membrane, and translucent cytoplasm. As the control, no obvious blue fluorescence emissions were observed from HeLa cells treated with Ir-DMSO alone (Figure S16). These results demonstrate that Ir-DMSO as a PS not only possessed effective PDT performance for cell apoptosis and necrosis under continuous light irradiation, but also had a self-reporting property for real-time monitoring therapeutic efficacy in a "signal on" mode without other signal probes.

To determine whether the PL emission enhancement comes from cellular His/His-containing proteins, experiments with DEPC-treated HeLa cells were conducted. The treatment of cells with DEPC can lead to the destruction of the cell membrane[27−29] and may cause cell death. When HeLa cells were treated with Ir-DMSO (10 μM) for 30 min after incubation with DEPC for 1 h, a bright red emission from PI and a weak blue emission from Ir-DMSO were simultaneously observed from PI-stained HeLa cells (Figure S17). Bright-field and merged images show that vacuoles fill up the entire cytoplasm and fragmented nucleus, indicating that these cells are dead. Also, there was no obvious blue emission from Ir-DMSO in these dead cells (Figure S17A). After treatment with His, these dead cells show strong blue and red fluorescence emissions (Figure S17B). On the other hand, strong blue emissions from HeLa cells treated with Ir-DMSO under light irradiation weaken evidently when DEPC was added under different conditions (Figure S18). These results suggest that

https://doi.org/10.1021/cbmi.4c00042
Chem. Biomed. Imaging 2024, 2, 808−816

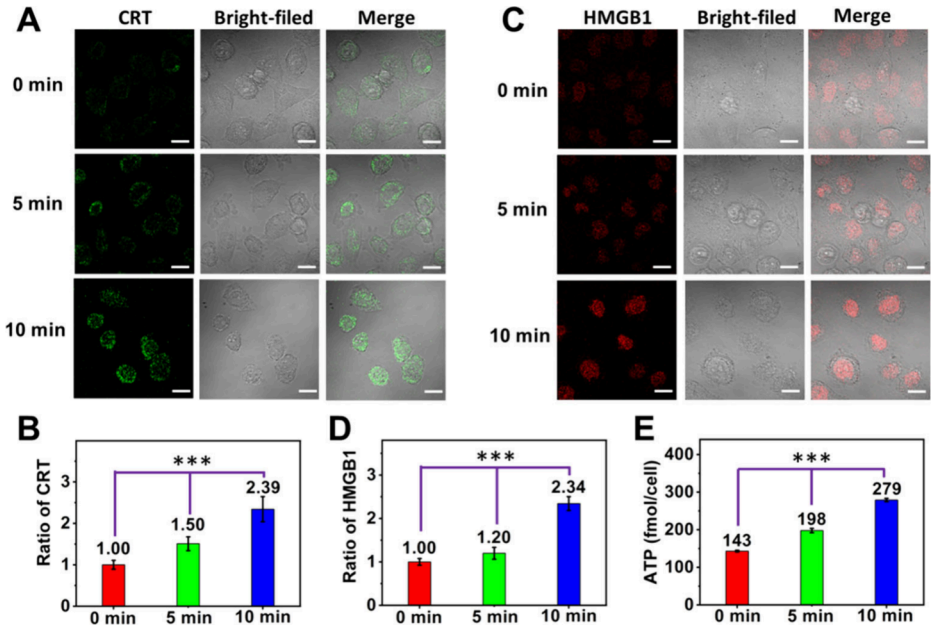

Figure 5. Evaluation for hallmarks of ICD in HeLa cells upon treatment with Ir-DMSO in the dark or upon white light irradiation. Immunofluorescence confocal laser scanning microscopy stained with (A) Alexa Fluor 488 conjugate calreticulin rabbit mAb and (C) Alexa Fluor 555 conjugate antirabbit IgG (H+L) and HMGB1 antibody. Analysis of CRT (B) and HMGB1 (D) levels in HeLa cells from (A) and (B). (E) Release of adenosine triphosphate into the cell culture supernatant. Probabilities $^{*}p < 0.05$, $^{**}p < 0.01$, $^{***}P < 0.001$ are marked in the figure and 0.05 was chosen as the significance level.

the enhanced blue PL signals during Ir-DMSO-induced PDT may be a result of intracellular His/His-containing proteins.

Therapeutic Mechanism of Ir-DMSO-Induced PDT

Inspired by the good self-reporting ability of Ir-DMSO in the PDT process with ROS generation and ER localization, the therapeutic mechanism of Ir-DMSO-induced PDT was investigated. Immunogenic cell death (ICD) is a cell death mechanism that activates the T-cell adaptive immunity, leading to the formation of long-term immunological memory.[30] ICD usually involves the translocation of the ER-resident calreticulin to the cell surface, the secretion of adenosine triphosphate, and the secretion of the nuclear high-mobility group box 1 protein.[30] These hallmarks were therefore investigated upon treatment of HeLa cells with Ir-DMSO and light irradiation. Using immunofluorescence confocal laser scanning microscopy, the translocation of CRT was observed (Figure 5A). Green fluorescence emissions can be seen from HeLa cells upon treatment with Ir-DMSO in the dark or under irradiation, indicating that CRT existed in the cytoplasm or the cell membrane (Figure 5A). Also, light irradiation results in a higher level of surface-exposed CRT (Figure 5B). In following, the possible migration of HMGB1 was monitored. As shown in Figure 5C, an increased trend of red fluorescence emissions with increasing irradiation time was observed for HeLa cells treated with Ir-DMSO, indicating the upregulation of HMGB1 during Ir-DMSO-induced PDT. The extracellular release of HMGB1 to the supernatant was quantified by an ELISA assay. A 2.34-fold enhancement of extracellular levels of HMGB1 was found upon exposure to light (Figure 5D). Futhermore, the release of ATP was studied using a specific bioluminescence detection kit. A nearly 2-fold increase in the extracellular ATP levels upon Ir-DMSO treatment under irradiation was observed (Figure 5E). There was no significant difference in the ratio of CRT or the ratio of HMGB1 calculated from HeLa cells in the same field of view and ATP content obtained from cell culture supernatant in six parallel experiments ($p > 0.05$), while there was extreme significant difference between ratio of CRT or ratio of HMGB1 calculated from HeLa cells upon different light irradiation times and ATP content obtained from cell culture supernatant in experimental groups under different light irradiation times ($p < 0.001$, Figure 5). These findings indicate that Ir-DMSO can trigger ICD upon visible light irradiation.

CONCLUSION

In summary, we have successfully designed and synthesized two nonemissive iridium(III) solvent complexes (Ir-DMSO and Ir-ACN) as PSs by introducing organic solvents into iridium(III) complexes as auxiliary ligands. Due to superior photophysical properties and lower cellular toxicity, Ir-DMSO was chosen for further PDT. Upon visible light irradiation, Ir-DMSO not only produces ROS to induce cell death but also presents the capacity of self-reporting therapeutic efficacy through a "signal on" mode. Further studies revealed that the "signal on" property of Ir-DMSO may result from its specific response to His/His-containing proteins. In addition, ICD was identified during Ir-DMSO-induced PDT, in which ROS generation, upregulation of surface-exposed CRT, and HMGB1 and ATP release were simultaneously observed. The limitation of Ir-DMSO is its strong blue-light absorption, which has poor tissue penetration. Future work will focus on near-infrared self-reporting PSs based on iridium(III) complexes. The work presented here provides a new and promising strategy for the development of self-reporting PS, which is of great importance for precise and effective PDT.

ASSOCIATED CONTENT

Supporting Information

The Supporting Information is available free of charge at https://pubs.acs.org/doi/10.1021/cbmi.4c00042.

https://doi.org/10.1021/cbmi.4c00042
Chem. Biomed. Imaging 2024, 2, 808−816

^{1}H NMR, ESI-HRMS spectra, crystal structure and data, PL emission spectra, colocalization experiments, and CLSM images of HeLa cells treated with different process in PDT process (PDF)

AUTHOR INFORMATION

Corresponding Authors

Honglan Qi − *Key Laboratory of Analytical Chemistry for Life Science of Shaanxi Province, School of Chemistry and Chemical Engineering, Shaanxi Normal University, Xi'an 710062, P. R. China;* orcid.org/0000-0002-2268-0073; Phone: +86−29−81530726; Email: honglanqi@snnu.edu.cn; Fax: +86−29−81530727

Meng Li − *Key Laboratory of Analytical Chemistry for Life Science of Shaanxi Province, School of Chemistry and Chemical Engineering, Shaanxi Normal University, Xi'an 710062, P. R. China*; Email: lemone@snnu.edu.cn

Authors

Manping Qian − *Key Laboratory of Analytical Chemistry for Life Science of Shaanxi Province, School of Chemistry and Chemical Engineering, Shaanxi Normal University, Xi'an 710062, P. R. China*

Ke Wang − *Key Laboratory of Analytical Chemistry for Life Science of Shaanxi Province, School of Chemistry and Chemical Engineering, Shaanxi Normal University, Xi'an 710062, P. R. China*

Peng Yang − *Key Laboratory of Analytical Chemistry for Life Science of Shaanxi Province, School of Chemistry and Chemical Engineering, Shaanxi Normal University, Xi'an 710062, P. R. China*

Yu Liu − *Key Laboratory of Analytical Chemistry for Life Science of Shaanxi Province, School of Chemistry and Chemical Engineering, Shaanxi Normal University, Xi'an 710062, P. R. China*

Chengxiao Zhang − *Key Laboratory of Analytical Chemistry for Life Science of Shaanxi Province, School of Chemistry and Chemical Engineering, Shaanxi Normal University, Xi'an 710062, P. R. China;* orcid.org/0000-0003-2829-5122

Complete contact information is available at: https://pubs.acs.org/10.1021/cbmi.4c00042

Author Contributions

#These authors contributed equally to this work.

Notes

The authors declare no competing financial interest.

ACKNOWLEDGMENTS

This work was supported by the National Natural Science Foundation of China (Nos. 22074087, 22374094, and 22274093) and the Fundamental Research Funds for the Central Universities (No. GK202202002).

REFERENCES

(1) Siegel, R. L.; Miller, K. D.; Jemal, A. Cancer Statistics. *Ca-Cancer J. Clin.* **2017**, *67*, 7−30.

(2) Karges, J.; Kuang, S.; Maschietto, F.; Blacque, O.; Ciofini, I.; Chao, H.; Gasser, G. Rationally Designed Ruthenium Complexes for 1- and 2-Photon Photodynamic Therapy. *Nat. Commun.* **2020**, *11*, 3262.

(3) Li, X.; Lee, S.; Yoon, J. Supramolecular Photosensitizers Rejuvenate Photodynamic Therapy. *Chem. Soc. Rev.* **2018**, *47*, 1174−1188.

(4) Shen, L.; Zhou, T.; Fan, Y.; Chang, X.; Wang, Y.; Sun, J.; Xing, L.; Jiang, H. Recent Progress in Tumor Photodynamic Immunotherapy. *Chin. Chem. Lett.* **2020**, *31*, 1709−1716.

(5) Chilakamarthi, U.; Giribabu, L. Photodynamic Therapy: Past, Present and Future. *Chem. Rec.* **2017**, *17*, 775−802.

(6) Correia, J. H.; Rodrigues, J. A.; Pimenta, S.; Dong, T.; Yang, Z. Photodynamic Therapy Review: Principles, Photosensitizers, Applications, and Future Directions. *Pharmaceutics* **2021**, *13*, 1332.

(7) Abramova, O. B.; Kozlovtseva, E. A.; Drozhzhina, V. V.; Ostroverkhov, P. V.; Sivovolova, T. P.; Arkhipova, L. M.; Grin, M. A.; Ivanov, S. A.; Kaprin, A. D. Anti-Tumor Efficacy of Photodynamic Therapy of Solid Tumors in Laboratory Animals with Guanidine and Biguanidine Derivatives of Chlorine *e6*. *B Exp. Biol. Med.* **2023**, *174*, 468−472.

(8) Reddy, M.; Bejoymohandas, K. Luminescent Lanthanide-based Molecular Materials: Applications in Photodynamic Therapy. *Dalton Trans.* **2024**, *53*, 1898−1914.

(9) Hu, X.; Wang, S.; Luo, Q.; Ge, B.; Cheng, Q.; Dong, C.; Xu, J.; Ding, H.; Xu, M.; Tedesco, A. C.; Huang, X.; Zhang, R.; Bi, H. Synthesis of Sn Nanocluster@carbon Dots for Photodynamic Therapy Application. *Chin. Chem. Lett.* **2021**, *32*, 2287−2291.

(10) Zhao, H.; He, M.; He, T.; Wu, Z.; Pan, Y.; Gao, J.; Miao, X.; Li, J.; Ma, H.; Huang, W.; Hu, W.; Fan, Q. Insights into the Excited State Dynamics of Donor-Acceptor Organic Photosensitizer for Precise Deep-Brain Two-Photon Photodynamic Therapy. *Laser Photonics. Rev.* **2024**, *18*, 2300917.

(11) Kuang, S.; Wei, F.; Karges, J.; Ke, L.; Xiong, K.; Liao, X.; Gasser, G.; Ji, L.; Chao, H. Photodecaging of a Mitochondria-Localized Iridium(III) Endoperoxide Complex for Two-Photon Photoactivated Therapy under Hypoxia. *J. Am. Chem. Soc.* **2022**, *144*, 4091−4101.

(12) Hou, M.; Chen, W.; Zhao, J.; Dai, D.; Yang, M.; Yi, C. Facile Synthesis and In Vivo Bioimaging Applications of Porphyrin Derivative-Encapsulated Polymer Nanoparticles. *Chin. Chem. Lett.* **2022**, *33*, 4101−4106.

(13) Sauraj; Kang, J. H.; Lee, O.; Ko, Y. T. Novel Aggregation-Induced Emission-Photosensitizers with Built-in Capability of Mitochondria Targeting and Glutathione Depletion for Efficient Photodynamic Therapy. *Nanoscale* **2023**, *15*, 4882−4892.

(14) Li, R.; Yang, T.; Peng, X.; Feng, Q.; Hou, Y.; Zhu, J.; Chu, D.; Duan, X.; Zhang, Y.; Zhang, M. Enhancing the Photosensitivity of Hypocrellin A by Perylene Diimide Metallacage-Based Host-Guest Complexation for Photodynamic Therapy. *Nano-Micro Lett.* **2024**, *16*, 226.

(15) Xiong, T.; Li, M.; Chen, Y.; Du, J.; Fan, J.; Peng, X. A Singlet Oxygen Self-Reporting Photosensitizer for Cancer Phototherapy. *Chem. Sci.* **2021**, *12*, 2515−2520.

(16) Wang, P.; Zhou, F.; Guan, K.; Wang, Y.; Fu, X.; Yang, Y.; Yin, X.; Song, G.; Zhang, X.; Tan, W. In Vivo Therapeutic Response Monitoring by a Self-Reporting Upconverting Covalent Organic Framework Nanoplatform. *Chem. Sci.* **2020**, *11*, 1299−1306.

(17) Zhang, T.; Li, Y.; Zheng, Z.; Ye, R.; Zhang, Y.; Kwok, R. T. K.; Lam, J. W. Y.; Tang, B. In Situ Monitoring Apoptosis Process by a Self-Reporting Photosensitizer. *J. Am. Chem. Soc.* **2019**, *141*, 5612−5616.

(18) Wang, D.; Chen, L.; Zhao, X.; Yan, X. A Unique Self-Reporting Photosensitizer Enabling Simultaneous Photodynamic Therapy and Real-Time Monitoring of Phototheranostic Process in a Dynamic Dual-Color Mode. *J. Mater. Chem. B* **2021**, *9*, 9900−9907.

(19) You, Y.; Park, S. Y. Inter-Ligand Energy Transfer and Related Emission Change in the Cyclometalated Heteroleptic Iridium Complex: Facile and Efficient Color Tuning over the Whole Visible Range by the Ancillary Ligand Structure. *J. Am. Chem. Soc.* **2005**, *127*, 12438−12439.

(20) Qian, M.; Zhang, D.; Qi, H.; Yang, X.; Yin, G.; Zhang, C.; Guo, J.; Qi, H. pH-Responsive Aldehyde-Bearing Cyclometalated Iridium-

(III) Complex for Tracking Intracellular pH Fluctuations Under External Stimulation. *Chin. Chem. Lett.* **2023**, *34*, 107336.
(21) Triesscheijn, M.; Baas, P.; Schellens, J. H. M.; Stewart, F. A. Photodynamic Therapy in Oncology. *Oncologist* **2006**, *11*, 1034−1044.
(22) Ma, D. L.; Wong, W.; Chung, W.; Chan, F.; So, P.; Lai, T.; Zhou, Z.; Leung, Y.; Wong, K. A Highly Selective Luminescent Switch-on Probe for Histidine/Histidine-rich Proteins and Its Application in Protein Staining. *Angew. Chem., Int. Ed.* **2008**, *47*, 3735−3739.
(23) Wang, H.; Han, L.; Zheng, D.; Yang, M.; Andaloussi, Y. H.; Cheng, P.; Zhang, Z.; Ma, S.; Zaworotko, M. J.; Feng, Y.; Chen, Y. Protein-Structure-Directed Metal-Organic Zeolite-Like Networks as Biomacromolecule Carriers. *Angew. Chem., Int. Ed.* **2020**, *59*, 6263−6267.
(24) Zhang, M.; Qian, M.; Huang, H.; Gao, Q.; Zhang, C.; Qi, H. Carboxyl Group Bearing Iridium(III) Solvent Complex as Photoluminescence and Electrochemiluminescence Probe for the Detection of Histidine. *J. Electroanal. Chem.* **2022**, *920*, 116578.
(25) Schweitzer, C.; Schmidt, R. Physical Mechanisms of Generation and Deactivation of Singlet Oxygen. *Chem. Rev.* **2003**, *103*, 1685−1758.
(26) Kamkaew, A.; Lim, S. H.; Lee, H. B.; Kiew, L. V.; Chung, L. Y.; Burgess, K. BODIPY Dyes in Photodynamic Therapy. *Chem. Soc. Rev.* **2013**, *42*, 77−88.
(27) Limpikirati, P.; Pan, X.; Vachet, R. W. Covalent Labeling with Diethylpyrocarbonate: Sensitive to the Residue Microenvironment, Providing Improved Analysis of Protein Higher Order Structure by Mass Spectrometry. *Anal. Chem.* **2019**, *91*, 8516−8523.
(28) Zhou, Y.; Vachet, R. W. Diethylpyrocarbonate Labeling for the Structural Analysis of Proteins: Label Scrambling in Solution and How to Avoid It. *J. Am. Soc. Mass Spectrom.* **2012**, *23*, 899−907.
(29) Mendoza, V. L.; Vachet, R. W. Protein Surface Mapping Using Diethylpyrocarbonate with Mass Spectrometric Detection. *Anal. Chem.* **2008**, *80*, 2895−2904.
(30) Alzeibak, R.; Mishchenko, T. A.; Shilyagina, N. Y.; Balalaeva, I. V.; Vedunova, M. V.; Krysko, D. V. J. Targeting Immunogenic Cancer Cell Death by Photodynamic Therapy: Past, Present and Future. *Immunother. Cancer* **2021**, *9*, No. e001926.

https://doi.org/10.1021/cbmi.4c00042
Chem. Biomed. Imaging 2024, 2, 808−816